Iterative Kramers-Kronig method for non-interferometric quantitative phase imaging: beyond the first-order Born and Rytov approximations

QIAN SHEN[1,2,3], JIASONG SUN[1,2,3], SHUN ZHOU[1,2,3], YAO FAN[1,2,3], ZHUOSHI LI[1,2,3], QIAN CHEN[3], MACIEJ TRUSIAK[4], MALGORZATA KUJAWINSKA[4], AND CHAO ZUO[1,2,3,*]

[1] *Smart Computational Imaging Laboratory (SCILab), School of Electronic and Optical Engineering, Nanjing University of Science and Technology, Nanjing, Jiangsu Province 210094, China*

[2] *Smart Computational Imaging Research Institute (SCIRI) of Nanjing University of Science and Technology, Nanjing, Jiangsu Province 210019, China*

[3] *Jiangsu Key Laboratory of Spectral Imaging & Intelligent Sense, Nanjing, Jiangsu Province 210094, China*

[4] *Warsaw University of Technology, Institute of Micromechanics and Photonics, 8 Sw. A. Boboli St., Warsaw 02-525, Poland*

[*] *zuochao@njust.edu.cn*

Compiled January 13, 2025

Traditional non-interferometric QPI methods often face challenges in realizing rapid and accurate imaging of large-phase samples, mainly due to slow convergence and dependence on object approximation models. In this Letter, we propose a new non-interferometric QPI approach that leverages iterative Kramers-Kronig (KK) relations, named iKK-QPI, to achieve high-accuracy quantitative measurement of objects with large phase values. In the current KK relations reconstruction framework, we impose real-part constraints on the cepstrum, breaking the restriction of weak scattering condition. With only a few iterations, iKK-QPI extends the phase range that can be reliably retrieved by non-interferometric QPI, exceeding the first-order Born and Rytov approximations. The capability of iKK-QPI is demonstrated by imaging a microlens array and COS-7 cells. We accurately reconstruct objects with large phase ranges 6 rad (error $< \pm 5\%$), three times that of the KK relations-based method, opening up the possibility for non-interferometric QPI to measure biological and industrial samples with large-phase features.

http://dx.doi.org/10.1364/ao.XX.XXXXXX

Quantitative phase imaging (QPI) has emerged as an essential optical tool in biological research and medical diagnostics owing to its capability to quantify the optical thickness of living cells and tissues in a label-free manner. The phase distribution allows the determination of cellular structure and biophysical parameters, which is crucial for the investigation of their intrinsic properties. [1, 2] Conventional QPI techniques generally rely on the superposition of two highly coherent beams, demanding complex interferometric configurations and stable environments. [3] Moreover, the interferometric characteristics lead to limited lateral resolution and laser speckle noise, prohibiting their widespread use in biological and medical science.

Non-interferometric QPI techniques address several issues inherent in interferometric methods, offering simplified imaging system while enhancing reconstruction accuracy and quality. These techniques recover the phase directly from the intensity, viewing it as an inverse problem that requires a rigorous "intensity-phase" model, which varies across different imaging systems. A coherent imaging system, such as Fourier ptychographic microscopy (FPM) [4–6], is linear in complex amplitude. Despite this, FPM still suffers from two weaknesses: (1) substantial data redundancy is required to ensure stable convergence; (2) a reliable solution needs considerable iterations and is computationally intensive. These limitations complicate the optimal balance between reconstruction speed and measurement precision, especially for objects with high phase dynamic range (referred to as "large-phase" objects below for brevity). In contrast, the nonlinear image generation model of partially coherent imaging leads to the coupling of amplitude and phase, such as transport of intensity equation (TIE) [7, 8] and differential phase contrast (DPC) [9, 10]. Their solutions often linearize the forward model of the imaging process by introducing the Born/Rytov (weak/slowly varying object) approximation. Specifically, the first-order Born approximation assumes that the object exhibits weak scattering [11], while the first-order Rytov approximation presumes that the phase gradient introduced by the object is relatively smooth [12]. The deterministicity of phase retrieval depends on these approximations, which are not always strictly valid in practical applications. Although some iterative methods can overcome these limitations, the solutions remain intricate and do not depart from the process of introducing approximate models [13]. Consequently, non-interferometric phase retrieval for samples with large phase values remains a challenge.

Recently, the Kramers-Kronig (KK) relations have garnered interest in QPI field [14–17] due to their distinctive ability to decouple the real and imaginary components of a complex function analytic in the upper half-plane. A method based on space-domain KK relations transforms the spatial intensity variations into spatial phase variations, allowing for phase images from a single intensity measurement under oblique illumination. [18] Essentially, the KK relations establish a linear model that converts a multiplicative modulation relationship into an additive one via cepstrum, a nonlinear operation that does not involve any object approximation. However, the true phase range remains unrecoverable solely relying on the KK relations when the object scattering is strong. Nevertheless, its linear model gets rid of the approximation limitations that usually conflict with the optical properties of samples, providing the potential to estimate the morphology of large-phase objects more accurately.

In this Letter, we propose an iterative KK relations-based method for non-interferometric QPI (iKK-QPI) to achieve high-accuracy large-phase retrieval, exceeding the limitations of the first-order Born and Rytov approximations. We use the KK relations to model objects and combine it with a complex amplitude retrieval process. This model uses the cepstrum to allow direct acquisition of analytical expression for intensity and phase without any approximation process, which avoids the nonlinear errors arising from the neglect of higher-order terms in Born or Rytov approximation. Furthermore, we update the real part of the complex amplitude in the logarithmic domain by iteration. iKK-QPI imposes constraints based on the KK relations to dramatically speed up the iterative convergence, enabling high-precision reconstruction with only a few iterations. Thus, the proposed method overcomes the challenge of applying non-interferometric QPI techniques to large-phase samples.

Conventional non-interferometric QPI methods commonly simplify the imaging model to a mathematical analytical form by introducing object approximations. However, these approximation conditions ignore a series of higher-order phase terms, leading to nonlinear errors. More importantly, accurate phase retrieval cannot be achieved for samples that deviate from these conditions, such as large-phase objects. In our method, instead of the approximate models that introduce higher-order nonlinear errors, iKK-QPI describes the distribution of objects by a more accurate linear imaging model based on the KK relations. To satisfy the KK relations, we use annular matched illumination [19], i.e., the unscattered light must be located at the edge of the pupil in the Fourier plane. The complex amplitude of the object under each illumination angle is $U_i(x,y)$, the sub-spectrum of the corresponding aperture is $S_i(u,v)$, and the captured intensity image is $I_i = |U_i(x,y)|^2$. Define a complex function

$$\chi(\mathbf{r}) = \log[U_i(\mathbf{r})] - i\mathbf{k}_{inc}\cdot\mathbf{r} \tag{1}$$

where $\mathbf{r} = x\hat{\mathbf{x}} + y\hat{\mathbf{y}}$, $\mathbf{k}_{inc}$ is the transverse wave vector of the incident plane wave. The imaginary part of $\chi(\mathbf{r})$ can be obtained from its real part $\mathrm{Re}[\chi(r)] = \log(I_i)/2$ by a directional Hilbert transform, and thus the complete complex amplitude of the object is reconstructed.

Assuming that the incident beam is a quasi-monochromatic plane wave $U_{in}(\mathbf{r}) = |U_{in}|\, e^{i\mathbf{k}_{inc}\cdot\mathbf{r}}$, the total field $U(\mathbf{r})$ can be regarded as a superposition of the incident field $U_{in}(\mathbf{r})$ and the scattered field $U_s(\mathbf{r})$, i.e., $U(\mathbf{r}) = U_{in}(\mathbf{r}) + U_s(\mathbf{r})$. Then the Eq. (1) can be written as

$$\chi = \log\left[1 + \frac{U_s}{U_{in}}\right] + \log|U_{in}| \tag{2}$$

Without loss of generality, the incident beam can be considered to have a unit amplitude $U_{in}(\mathbf{r}) = e^{i\mathbf{k}_{inc}\cdot\mathbf{r}}$, then the intensity and scattered field can be transformed into an additive relationship by the cepstrum

$$\log I = \log(1 + U_s) + \log(1 + U_s)^* \tag{3}$$

Different from the Born/Rytov approximation, the equality sign of Eq. (3) always holds without any approximation. For $|U_{in}| > |U_s|$, the logarithmic term in Eq. (2) can be Taylor expanded as

$$\log\left[1 + \frac{U_s}{U_{in}}\right] = \sum_{n=0}^{\infty} \frac{(-1)^n}{n+1}\left(\frac{U_s}{U_{in}}\right)^{n+1} \tag{4}$$

Since the analyticity means the existence of a convergent power series, the validity of the KK relations requires that the unscattered light is stronger than the scattered light. Due to the intrinsic correlation between the scattering intensity and the internal refractive index variations of the object, which manifest as phase changes in QPI, the fulfillment of this condition is closely related to the phase distribution of the measured object. For large-phase objects with strong scattering, the higher-order power series in Eq. (4) are severely divergent in the frequency domain, making reconstruction via the KK relations no longer valid [Fig. 1(a)]. In addition, the phase gradient is also one of the crucial factors in determining the reconstruction quality. For the same phase range, smaller phase gradient means higher reconstruction accuracy [Fig. 1(b)]. Inspired by the alternating projection in phase retrieval, an iterative algorithm based on the KK relations model enables high-accuracy reconstruction of objects with large phase values and phase gradients through nonlinear optimization.

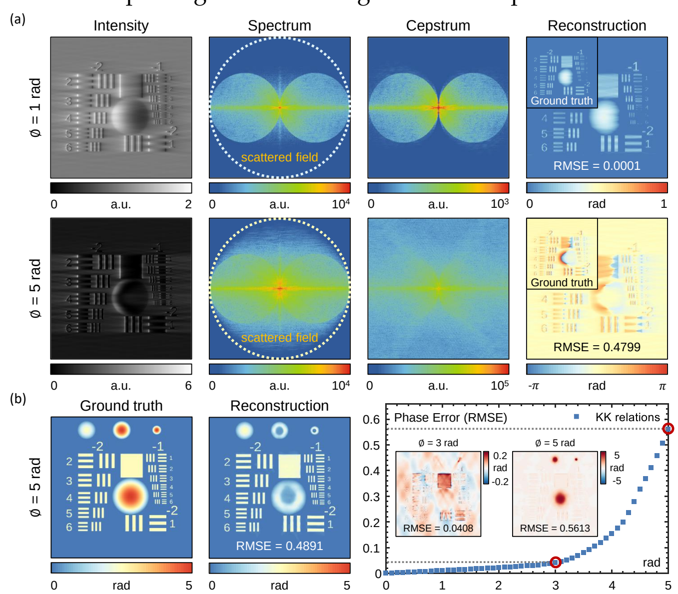

Fig. 1. Simulation results of the KK relations-based method. (a) Comparison of intensity, spectrum and reconstruction results for objects of different phase ranges. (b) Reconstruction result of a 5 rad object and RMSE curve as phase increases.

Figure 2 illustrates the working flow of iKK-QPI with unstained COS-7 cells as an example. Multi-angle intensity images are acquired under the matched illumination condition and the complex amplitude of the object is reconstructed via the KK relations [see Step1]. In Step2, we take the reconstructed complex amplitude as the initial value to perform the iteration. Taking the logarithm of $U_i(x,y)$ corresponding to the sub-spectrum $S_i(u,v)$ of each illumination angle in turn, we obtain $\log[U_i(x,y)]$, whose complex amplitude can be written in the form of $A + iB$, with A and B denoting the real and imaginary parts. According to Eq. (3), calculate $\log(I_i)/2$ and update the real part A. One iteration of the algorithm is completed after updating all the sub-spectrums. This process is repeated to minimize the L_2- distance between the real part of the logarithm of forward-generated complex amplitude and the logarithm of observations until convergence. The reconstructed phase range is much larger than the initial value via the KK relations [see Step 3]. It should be emphasized that the intensity constraint of iKK-QPI is conducted in the logarithmic domain, which is a fundamental difference from conventional FPM. The details of high and low brightness regions in a logarithmic image can be displayed simultaneously. In addition, the logarithmic operation combined with filtering can suppress the effects of noise, particularly multiplicative noise, thereby improving the image quality. [20] iKK-QPI achieves high-precision measurement of large-phase objects with only a few iterations, enhancing the imaging efficiency of large-phase objects.

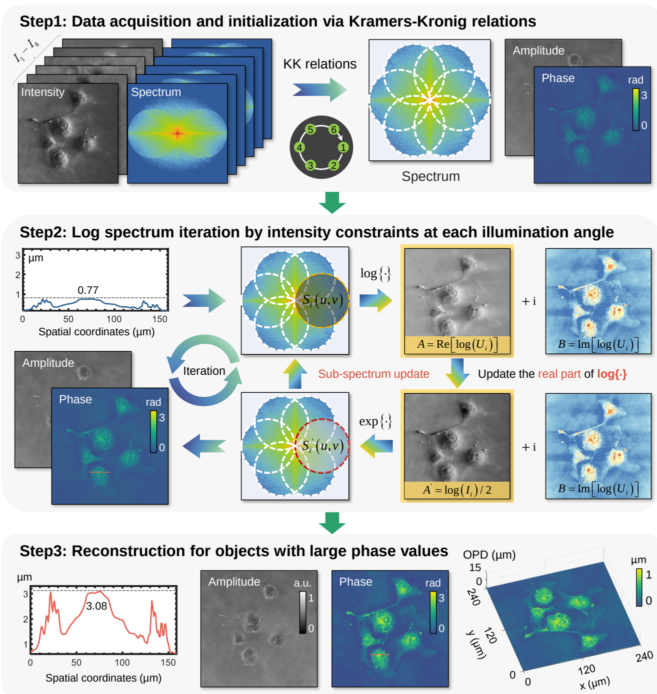

Fig. 2. Flow chart of data processing in iKK-QPI for large-phase retrieval on the example of unstained COS-7 cells.

Simulations were carried out to verify the validity of iKK-QPI for reconstructing large-phase objects. We simulated a sample with a phase distribution of $0 - 5$ rad [Fig. 3(a)], in which the scattered light is stronger than the unscattered light, exceeding the typical conditions required for accurate phase retrieval with the KK relations. As a result, the phase reconstructed by the KK relations-based method exhibits a much smaller range than the true value, leading to errors in the amplitude at the same positions [Fig. 3(b)]. We solved the phase using FPM and iKK-QPI, respectively, where the conventional FPM algorithm takes the average value of the intensity images as the initialization. The root mean square error (RMSE) curves for the two iterative methods are shown in Fig. 3(c). It is obvious from the blue curve that as the number of iterations increases, the RMSE value of iKK-QPI decreases rapidly and finally converges to 0 after just 5 iterations (RMSE 0.0112, total computation time 0.6 s with a 2.60 GHz laptop). In contrast, FPM requires 15 iterations to reduce the RMSE evidently (red curve), three times as many as iKK-QPI. Even after 15 iterations (RMSE 0.0757, total computation time 1.9 s), the reconstruction results of FPM still suffered from severe errors and thus could not be correctly phase unwrapped, resulting in distortion of the object shape [Fig. 3(d)]. iKK-QPI reconstructed large-phase objects with high accuracy in just 5 iterations, as shown by the amplitude and unwrapped phase results in Fig. 3(e). In addition, we performed 20 experiments under varying signal-to-noise ratios (SNRs) to evaluate the performance of the two methods, confirming the noise suppression capability of iKK-QPI [Fig. 3(f)].

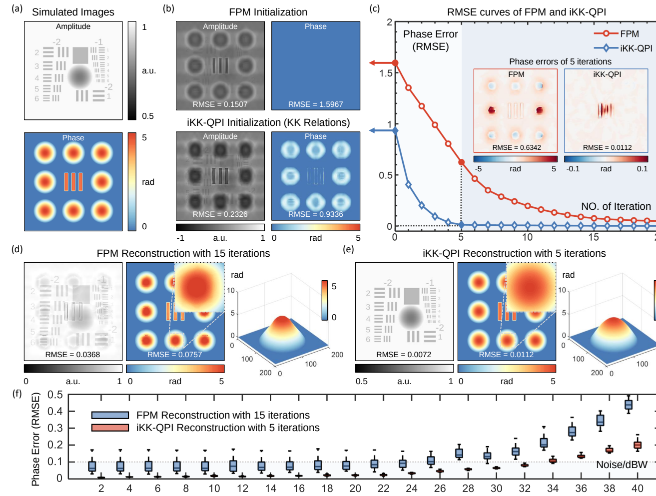

Fig. 3. Simulation results of FPM and iKK-QPI for large-phase samples. (a) The simulated images. (b) Initialization. (c) RMSE curves versus the iteration number. (d), (e) Reconstruction results. (f) Phase error of reconstruction at different SNRs.

To verify the practicality of iKK-QPI, two experiments were performed with the imaging system of AIFPM [19]. We used a programmable LED array to implement the annular illumination scheme. The height of the LED array is adjusted to position each LED element precisely at the edge of the objective numerical aperture (NA) in frequency space, ensuring that the KK relations hold. The pixel size of the CMOS camera is 2.4 μm, and the central wavelength of the illumination is 550 nm.

To quantitatively demonstrate the accuracy of iKK-QPI for large-phase retrieval, we imaged a standard microlens array with a curvature radius of 500 μm and a pitch of 75 μm. Its theoretical height is around 1.2 μm, corresponding to a phase amplitude of 6 rad. We used an objective lens with ×4/0.16NA (Olympus UPlanSApo) and acquired 8 images under annular matched illumination. Since the background of the sample carries absorption, we processed the reconstructed phase with a mask. The results of the KK relations-based method presented considerably weaker phase contrast, indicating that the phase range was much smaller than the theoretical value [Fig. 4(a)]. iKK-QPI reconstructed a highly accurate phase distribution with only 5 iterations, while FPM failed to obtain the correct results even after 15 iterations [Fig. 4(b) and (c)]. From the three-dimensional (3D) pseudo-color morphology in Fig. 4(e), iKK-QPI characterizes the true morphology of the microlens. To quantitatively assess the measurement precision, the same sample was measured using a custom-built digital holographic microscope (DHM) equipped with a ×10/0.4 NA objective lens (laser wavelength 550 nm) [Fig. 4(d)]. After phase unwrapping and converting to physical thickness, one microlens unit was selected and the phase values along the white dashed line were plotted in Fig. 4(f). Although the curvature radius of this line profile of DHM after arch fitting reached an acceptable agreement with the nominal value, it suffered severely from noise. The results obtained by iKK-QPI with 5 iterations are almost the same as the true value (error $< \pm 5\%$). It verifies that iKK-QPI realizes high-accuracy reconstruction of large-phase objects and provides reliable quantitative phase data for subsequent research and analysis.

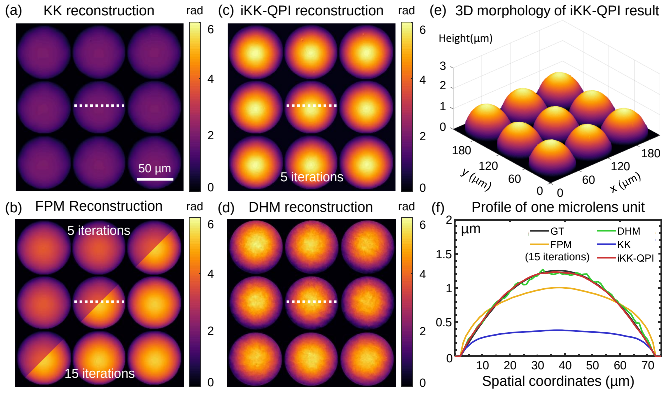

Fig. 4. Comparative experiments on a standard microlens array sample. (a)–(d) Reconstructed phase distribution separately based on the KK relations, FPM, iKK-QPI, and DHM methods. (e) 3D pseudo-color morphological distribution. (f) Quantitative phase values along the white dashed.

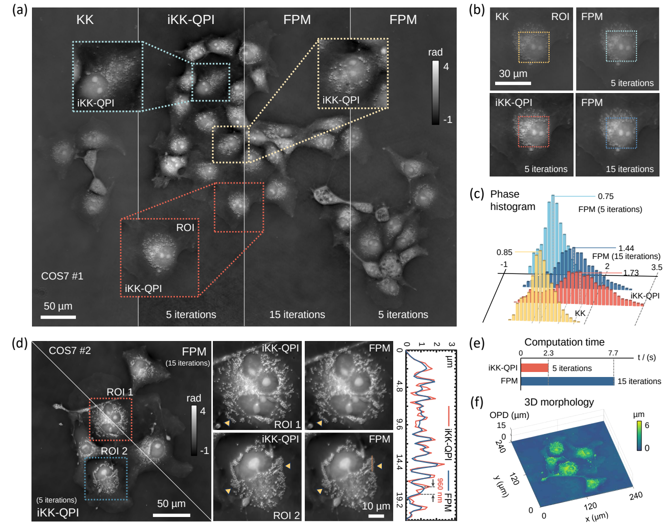

Fig. 5. Comparative experiments on COS-7 cells. (a) Reconstructed phase under the KK relations, iKK-QPI and FPM. (b) Enlarged images of the area in the red box in (a). (c) Phase histogram of the boxed regions in (b). (d) Reconstructed phase with iKK-QPI (5 iterations) and FPM (15 iterations), and phase values along the red line. (e) Computation time for the results in (d). (f) 3D display of reconstruction results.

Experiments on a COS-7 cell sample was conducted to demonstrate the capability of iKK-QPI for imaging complex samples such as unlabeled cells. We switched to a ×10/0.4NA objective lens to better visualize cellular details. The phase results are shown in Fig. 5(a). It is evident that the reconstruction results of different methods are roughly the same for the relatively thin regions of the cells, but the phase values for the thicker regions around the nucleus differ considerably. The phase range reconstructed using the KK relations-based method is approximately 2.5 rad, much smaller than the theoretical thickness of COS-7 cells. In consistent with the simulation, iKK-QPI reconstructed 4 rad in only 5 iterations, while FPM was still not reached in 15 iterations. We selected a cell [Fig. 5(b)] and calculated the histograms of the dashed box regions, as shown in Fig. 5(c). The histograms provide a direct visualization of the phase distribution, further illustrating the effectiveness of the proposed method for large-phase retrieval. In addition, we compared the reconstructed image quality of iKK-QPI and FPM with two regions of interest (ROI) as shown in Fig. 5(d). Although both methods obtained similar phase ranges, iKK-QPI reconstructed COS-7 cells with much sharper edges of organelles such as nuclei and lipid droplets, even increasing the resolution. Moreover, the reconstruction process of iKK-QPI substantially reduced the number of iterations and shortened the time by more than three-fold compared with FPM [Fig. 5(e)]. This experiment demonstrated that iKK-QPI provides higher reconstruction accuracy and quality in shorter time for large-phase retrieval.

In conclusion, we have proposed the iKK-QPI method for high-accuracy imaging of large-phase objects. By integrating the KK relations with the real-part constraint of the cepstrum, iKK-QPI has overcome the limitations of conventional QPI technique for measuring large-phase objects, significantly broadening the application of QPI. This method belongs to the non-interferometric QPI technique, which does not require complex interferometric setups and coherent illumination, making it less susceptible to noise and artifacts. Experimental validation with a microlens array and live COS-7 cells has demonstrated the practical applicability of iKK-QPI, providing a promising tool for quantitative morphological measurements in both biological research and industrial inspection. In the future, iKK-QPI is expected to be combined with deep learning [21, 22], giving the potential to further enhance the imaging performance of non-interferometric QPI. iKK-QPI can also be extended to diffraction tomography for measuring 3D refractive index distribution of transparent samples [23–25], opening up new possibilities for studying a diverse range of specimens in various scientific fields.

Funding. National Natural Science Foundation of China (62227818, 62361136588), National Key Research and Development Program of China (2022YFA1205002, 2024YFE0101300), Key National Industrial Technology Cooperation Foundation of Jiangsu Province (BZ2022039), China Postdoctoral Science Foundation (2023TQ0160, 2023M731683), and National Science Center, Poland (2023/48/Q/ST7/00172).

Disclosures. The authors declare no conflicts of interest.

REFERENCES

1. Y. Park, C. Depeursinge, and G. Popescu, Nat. photonics **12**, 578 (2018).
2. Z. Huang and L. Cao, Light. Sci. & Appl. **13**, 145 (2024).
3. E. Cuche, F. Bevilacqua, and C. Depeursinge, Opt. letters **24**, 291 (1999).
4. G. Zheng, R. Horstmeyer, and C. Yang, Nat. photonics **7**, 739 (2013).
5. X. Ou, G. Zheng, and C. Yang, Opt. express **22**, 4960 (2014).
6. C. Zuo, J. Sun, and Q. Chen, Opt. express **24**, 20724 (2016).
7. M. R. Teague, JOSA **73**, 1434 (1983).
8. C. Zuo, J. Li, J. Sun, *et al.*, Opt. Lasers Eng. **135**, 106187 (2020).
9. S. B. Mehta and C. J. Sheppard, Opt. letters **34**, 1924 (2009).
10. L. Tian and L. Waller, Opt. express **23**, 11394 (2015).
11. J. M. Cowley, *Diffraction physics* (Elsevier, 1995).
12. M. H. Jenkins and T. K. Gaylord, Appl. optics **54**, 8566 (2015).
13. Y. Fan, J. Sun, Y. Shu, *et al.*, Photonics Res. **11**, 442 (2023).
14. C. Shen, M. Liang, A. Pan, and C. Yang, Photonics Res. **9**, 1003 (2021).
15. Z. Huang and L. Cao, Adv. Photonics Res. **3**, 2100273 (2022).
16. R. Cao, C. Shen, and C. Yang, Nat. Commun. **15**, 4713 (2024).
17. S. Zhao, H. Zhou, S. Lin, *et al.*, Biomed. Opt. Express **15**, 5739 (2024).
18. Y. Baek and Y. Park, Nat. Photonics **15**, 354 (2021).
19. J. Sun, C. Zuo, J. Zhang, *et al.*, Sci. reports **8**, 7669 (2018).
20. R. C. Gonzales and P. Wintz, *Digital image processing* (Addison-Wesley Longman Publishing Co., Inc., 1987).
21. A. Saba, C. Gigli, A. B. Ayoub, and D. Psaltis, Adv. Photonics **4**, 066001 (2022).
22. Z. Wu, I. Kang, Y. Yao, *et al.*, eLight **3**, 7 (2023).
23. C. Zuo, J. Sun, J. Li, *et al.*, Opt. Lasers Eng. **128**, 106003 (2020).
24. J. Li, N. Zhou, J. Sun, *et al.*, Light. Sci. & Appl. **11**, 154 (2022).
25. Z. Huang and L. Cao, APL Photonics **9** (2024).

FULL REFERENCES

1. Y. Park, C. Depeursinge, and G. Popescu, "Quantitative phase imaging in biomedicine," Nat. photonics **12**, 578–589 (2018).
2. Z. Huang and L. Cao, "Quantitative phase imaging based on holography: trends and new perspectives," Light. Sci. & Appl. **13**, 145 (2024).
3. E. Cuche, F. Bevilacqua, and C. Depeursinge, "Digital holography for quantitative phase-contrast imaging," Opt. letters **24**, 291–293 (1999).
4. G. Zheng, R. Horstmeyer, and C. Yang, "Wide-field, high-resolution fourier ptychographic microscopy," Nat. photonics **7**, 739–745 (2013).
5. X. Ou, G. Zheng, and C. Yang, "Embedded pupil function recovery for fourier ptychographic microscopy," Opt. express **22**, 4960–4972 (2014).
6. C. Zuo, J. Sun, and Q. Chen, "Adaptive step-size strategy for noise-robust fourier ptychographic microscopy," Opt. express **24**, 20724–20744 (2016).
7. M. R. Teague, "Deterministic phase retrieval: a green's function solution," JOSA **73**, 1434–1441 (1983).
8. C. Zuo, J. Li, J. Sun, *et al.*, "Transport of intensity equation: a tutorial," Opt. Lasers Eng. **135**, 106187 (2020).
9. S. B. Mehta and C. J. Sheppard, "Quantitative phase-gradient imaging at high resolution with asymmetric illumination-based differential phase contrast," Opt. letters **34**, 1924–1926 (2009).
10. L. Tian and L. Waller, "Quantitative differential phase contrast imaging in an led array microscope," Opt. express **23**, 11394–11403 (2015).
11. J. M. Cowley, *Diffraction physics* (Elsevier, 1995).
12. M. H. Jenkins and T. K. Gaylord, "Quantitative phase microscopy via optimized inversion of the phase optical transfer function," Appl. optics **54**, 8566–8579 (2015).
13. Y. Fan, J. Sun, Y. Shu, *et al.*, "Accurate quantitative phase imaging by differential phase contrast with partially coherent illumination: beyond weak object approximation," Photonics Res. **11**, 442–455 (2023).
14. C. Shen, M. Liang, A. Pan, and C. Yang, "Non-iterative complex wave-field reconstruction based on kramers–kronig relations," Photonics Res. **9**, 1003–1012 (2021).
15. Z. Huang and L. Cao, "High bandwidth-utilization digital holographic multiplexing: an approach using kramers–kronig relations," Adv. Photonics Res. **3**, 2100273 (2022).
16. R. Cao, C. Shen, and C. Yang, "High-resolution, large field-of-view label-free imaging via aberration-corrected, closed-form complex field reconstruction," Nat. Commun. **15**, 4713 (2024).
17. S. Zhao, H. Zhou, S. Lin, *et al.*, "Efficient, gigapixel-scale, aberration-free whole slide scanner using angular ptychographic imaging with closed-form solution," Biomed. Opt. Express **15**, 5739–5755 (2024).
18. Y. Baek and Y. Park, "Intensity-based holographic imaging via space-domain kramers–kronig relations," Nat. Photonics **15**, 354–360 (2021).
19. J. Sun, C. Zuo, J. Zhang, *et al.*, "High-speed fourier ptychographic microscopy based on programmable annular illuminations," Sci. reports **8**, 7669 (2018).
20. R. C. Gonzales and P. Wintz, *Digital image processing* (Addison-Wesley Longman Publishing Co., Inc., 1987).
21. A. Saba, C. Gigli, A. B. Ayoub, and D. Psaltis, "Physics-informed neural networks for diffraction tomography," Adv. Photonics **4**, 066001–066001 (2022).
22. Z. Wu, I. Kang, Y. Yao, *et al.*, "Three-dimensional nanoscale reduced-angle ptycho-tomographic imaging with deep learning (rapid)," eLight **3**, 7 (2023).
23. C. Zuo, J. Sun, J. Li, *et al.*, "Wide-field high-resolution 3d microscopy with fourier ptychographic diffraction tomography," Opt. Lasers Eng. **128**, 106003 (2020).
24. J. Li, N. Zhou, J. Sun, *et al.*, "Transport of intensity diffraction tomography with non-interferometric synthetic aperture for three-dimensional label-free microscopy," Light. Sci. & Appl. **11**, 154 (2022).
25. Z. Huang and L. Cao, "k-space holographic multiplexing for synthetic aperture diffraction tomography," APL Photonics **9** (2024).